Transient Voltage Characteristics and Support Strategy of Hybrid Cascaded HVDC System Under Sending-end AC System Fault

Jiangshan Liu, Fengting Li, Chunya Yin, *Member*, *IEEE*, Lu Han, Gaohang Zhang, Ruikang Chen, and Wan Liu

***Abstract*—During sending-end faults in the hybrid cascaded HVDC (HC-HVDC) system, the transient voltage drop characteristics under the interaction of the AC/DC hybrid system remain unclear, and the reactive power support provided by the HC-HVDC to the sending-end AC system requires further investigation. To address this problem, the reactive power interaction coupling mechanism between the sending-end AC system and the HC-HVDC is revealed, and the transient voltage mathematical model considering fault severity and duration is established. Under the dynamic change of the AC system voltage, the difference between the reactive power provided only by the reactive power compensation devices and by the combined modular multilevel converters (MMC) and reactive power compensation devices is analyzed. It is concluded that using MMC to provide a proportion of reactive power enhances the reactive power support to the AC system during faults. Then, the transient voltage model considering the reactive power support of MMC is established, and the critical reactive power consumption of line commutated converter (LCC) is quantified. It is concluded that the reactive power consumption of LCC exceeding its critical value deteriorates the transient voltage. A coordinated support strategy for the sending-end AC system based on reactive power support of MMC and reactive power regulation of LCC is proposed. It can effectively address the challenge of weakened reactive power support to the AC system due to voltage drop, thereby preventing the unbalanced reactive power from deteriorating the transient voltage, and realizing active support of the transient voltage. Finally, a simulation model is established on the PSCAD/EMTDC platform, and the simulation results validate the effectiveness of the proposed strategy in supporting the transient voltage, under different fault types, durations, severities, and locations.**

Received: February 14, 2025
Accepted: October 22, 2025
Published Online: January 1, 2026
Jiangshan Liu, Fengting Li (corresponding author), Chunya Yin, Lu Han, Gaohang Zhang, Ruikang Chen, and Wan Liu are with the School of Electrical Engineering, Xinjiang University, Urumqi 830017, China (e-mail: xjdxljs@foxmail.com; 2286066579@qq.com; 1399132297@qq.com; 1119642065@qq.com; xjuzgh@xju.edu.cn; 809959388@qq.com; 1551992895@qq.com).
DOI: 10.23919/PCMP.2025.000097

***Index Terms*—Hybrid cascaded HVDC, transient voltage, cooperative control, reactive power.**

NOMENCLATURE

A. Abbreviations

LCC	line commutated converter
MMC	modular multilevel converters
HC-HVDC	hybrid cascaded HVDC system
VDCOL	voltage-dependent current order limiter

B. Variables

U_{dr}, U_{di}	DC voltages of rectifier and inverter
U_{dcMMC}	DC voltage of rectifier MMCs
U_{dcLCC}	DC voltage of rectifier LCC
U_{dcLCC0}	no-load DC voltage of LCC
I_{dc}	total DC current of rectifier
I_{dcMMCm}	DC current of each MMC
R_d	DC line equivalent resistance
N	number of six-pulse converters
T_r	transformation ratio of rectifier transformer
α_r	firing angle of rectifier LCC
X_{cr}	commutation reactance of rectifier LCC
P_{ac}, Q_{ac}	exchange active power and reactive power between AC and DC systems
Q_{acN}	rated reactive power between AC and DC systems
P_{HC}	active power of HC-HVDC
P_{LCC}	active power of rectifier LCC
P_{MMCm}	active power of each rectifier MMC
Q_{Cr}, Q_{CrN}	reactive power and rated reactive power of AC filter and capacitor in rectifier station
Q_{HC}	reactive power consumed by HC-HVDC rectifier
Q_{MMCm}	reactive power consumed by each rectifier MMC
P_{MMC}, Q_{MMC}	active power and reactive power for all rectifier MMCs

$Q_{\text{ref}m}$	reactive power order of each rectifier MMC
Q_{LCC}	reactive power consumed by rectifier LCC
φ_{r}	power factor angel of rectifier LCC
U_{Lr}, $U_{\text{Lr,pu}}$	line to line voltages of rectifier converter bus and converter bus voltage in per unit
$U_{\text{Lr,puN}}$	per-unit value of rated value of converter bus voltage
U_{LrN}	the rated converter bus of rectifier
Q_{acN}	rated exchange reactive power between AC and DC systems
ΔQ_{r}	unbalanced reactive power inject into sending-end AC system
ζ_{SCR}	short circuit ratio
P_{dN}	rated active power of DC system
S_{cr}	short circuit capacity of sending side AC system
$U_{\text{Lr,puf}}$	converter bus voltage caused by AC system fault
ΔU_{fq}	voltage variation caused by unbalanced reactive power
t_{f}	fault occurrence time
t_{dur}	fault duration
Q'_{Cr}	reactive power provided by AC filter and reactive power compensation devices under MMC reactive power support.
Q'_{CrN}	rated reactive power provided by AC filter and reactive power compensation devices under MMC reactive power support.
S_{MMC}	capacity of each MMC
$P_{\text{ref}m}$	active power reference of each MMC
m	number of MMCs
$U'_{\text{Lr,pu}}$	transient voltage under MMC reactive power support
Q^*_{LCC}	critical LCC reactive power consumption
I^*_{dc}	critical DC current
I^*_{dcref}	critical DC current order

I. Introduction

U-HVDC systems can realize large-scale, long-distance, and low-loss power transmission, and are widely used in the world [1]. However, as the development, utilization, and grid integration of new energy continue to expand, issues such as the weakening support role of conventional power sources and the decline in AC system strength become increasingly prominent [2], thereby reducing the adaptability of line commutated converter (LCC) HVDC. The sending-end hybrid cascaded HVDC (HC-HVDC) system consists of parallel modular multilevel converters (MMCs) in series with a LCC, offering economic efficiency, flexible control capability, and strong adaptability to weak networks [3]. The use of HC-HVDC at the sending-end is well suited to future power systems with an ultra-high share of new energy and holds broad application prospects [4]. However, in the event of faults at the sending-end, the active and reactive power between AC and DC systems change dramatically due to the strong coupling between the two systems [5], resulting in voltage drop [6] and threatening the safe and stable operation of the sending-end system. Therefore, it is urgent to investigate the transient voltage characteristics caused by faults occurring near the HC-HVDC sending-end system and to develop an effective transient voltage support strategy.

Existing research on HC-HVDC has been mainly aimed at the inverter. Application of HC-HVDC in the inverter side is proposed in [7], and the power operation range of HC-HVDC is established. The response characteristics of HC-HVDC with master-slave control and droop control are studied in [8] and [9], whereas the influence mechanism of AC system strength on the stability of HC-HVDC is further studied in [10]. However, since the inverter uses thyristors, it suffers the risk of commutation failure. Reactive power characteristic during commutation failure and its recovery are analyzed in [11]. In [12], it demonstrates that HC-HVDC has the ability of safe and stable operation under extremely weak synchronous support conditions, and has unique advantages when applying to sending-end systems with high proportion of new energy. References [13] and [14] further clarify the power characteristics of HC-HVDC in sending-end, and propose an active and reactive power support scheme. However, due to the specific HC-HVDC topology and the complexity of control, there are strong coupling characteristics between LCC, MMC and AC systems. The dynamic response characteristics of different types of converters vary under DC near-area AC system faults. However, the interaction mechanism between AC and DC systems remains unclear, making it challenge to analyze the transient voltage variations on the converter bus.

The research on the transient voltage characteristics of the sending-end AC system focuses on the transient overvoltage caused by the DC fault. Reference [15] clarifies the impact of the DC system on the AC system following a DC fault, while reference [16] analyzes the mechanism of transient overvoltage and establishes its calculation method. The calculation method of transient overvoltage considering the influence of transient characteristics of high proportion of new energy sources is further developed in [17]. In [18], the response characteristics of the HC-HVDC system at the sending-end

after commutation failure are studied, the mechanism of transient overvoltage is analyzed, and the differences between the system and the traditional DC transient overvoltage are compared and analyzed. In [19], the transient voltage characteristics caused by faults in the sending-end AC system are investigated, focusing on the control response characteristics of the DC system under different fault severities and its impact on the converter bus voltage. In [6], the mechanism of transient overvoltage during the recovery period of commutation failure caused by the sending-end AC system faults is studied, whereas in [20], the mechanism of transient overvoltage considering the interaction of active and reactive power under sending-end AC system faults is further analyzed.

The transient voltage regulation strategy mainly focuses on transient overvoltage suppression. In [21], by optimizing the voltage-dependent current order limiter (VDCOL) parameters, the reactive power exchange between the AC and DC systems [22] is adjusted to suppress transient overvoltage. The transient voltage suppression strategy considering the cooperative control of new energy units and DC system is further proposed in [23] and [24]. Reference [25] proposes to suppress transient overvoltage by adding fast response flexible reactive power compensation devices. In [6], a strategy of adjusting the early inverter firing angle is proposed to suppress the transient overvoltage in the fault recovery stage of the AC system at the sending-end, whereas a transient voltage suppression strategy considering active power support is proposed in [20].

The existing studies primary focus on transient overvoltage and its suppression strategy. However, there is a strong coupling between AC and DC systems after sending-end AC system faults, while there is limited research on the mechanism of transient voltage evolution considering the coupling between multi-type converters and the AC/DC systems. Therefore, identifying the components and dominant factors of transient voltage, and fully exploring the voltage support capabilities of LCC and MMC, are essential for addressing transient voltage issues.

The main contributions of this paper are listed as follows.

1) Considering the fault duration and severity, the expression of transient voltage caused by the sending-end AC system faults under strong AC/DC coupling is established. Fault severity, fault duration, and unbalanced reactive power are the main factors influencing the transient voltage, indicating that unbalanced reactive power can exacerbate the transient voltage caused by sending-end AC system faults.

2) Considering the transient and steady-state response characteristics of multiple converter types, a transient voltage expression considering MMC reactive power support is established, and the influence of LCC reactive power consumption on transient voltage is analyzed. An active support strategy for the sending-end AC system, based on LCC and MMC cooperative control, is proposed to prevent unbalanced power from deteriorating transient voltage and to provide active transient voltage support.

The remainder of this paper is organized as follows. In Section II, the topology and basic control strategy of HC-HVDC in sending-end are proposed. In Section III, the mechanism and calculation method of transient voltage considering different fault severities and durations are proposed, and its influencing factors are clarified. In Section IV, the transient voltage characteristics considering the reactive power support of MMC are analyzed, and the system power balance points are established. A transient voltage active support strategy based on LCC and MMC cooperative control is further proposed. In Section V, PSCAD/EMTDC simulation is conducted to verify the voltage support strategy with different case studies. In Section VI, the applicability of the proposed voltage support strategy is discussed, while Section VII concludes this paper.

II. Introduction to HC-HVDC in Sending-End System

A. HC-HVDC Topology

The sending-end HC-HVDC is composed of n sets of MMCm ($m = 1, 2, \cdots, n$) in parallel and a set of 12-pulse LCC in series, while a set of double 12-pulse LCC is used in the inverter side. The equivalent circuit of a typical HC-HVDC in sending-end is shown in Fig. 1.

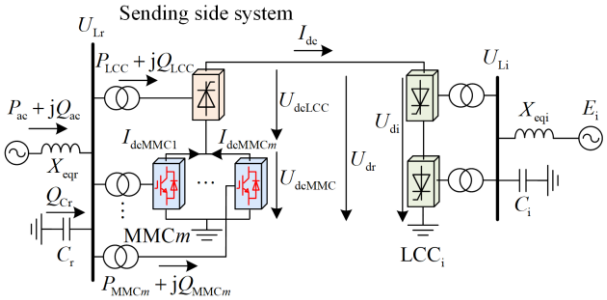

Fig. 1. Typical HC-HVDC in rectifier side.

When the HC-HVDC in Fig. 1 operates under normal conditions, the variables of the system are balanced. U_{dr} can be expressed as:

$$U_{dr}=U_{dcMMC}+U_{dcLCC} \tag{1}$$

where U_{dcLCC} can be expressed as:

$$\begin{cases} U_{dcLCC}=\dfrac{3\sqrt{2}}{\pi}NT_rU_{Lr}\cos\alpha_r-\dfrac{3}{\pi}NX_{cr}I_{dc} \\ I_{dc}=\sum_{m=1}^{n}I_{dcMMCm}=\dfrac{U_{dr}-U_{di}}{R_d} \end{cases} \tag{2}$$

The active and reactive power can be expressed as:

$$\begin{cases} P_{\mathrm{ac}} = P_{\mathrm{HC}} = P_{\mathrm{LCC}} + \sum_{m=1}^{n} P_{\mathrm{MMC}m} \\ Q_{\mathrm{ac}} + Q_{\mathrm{Cr}} = Q_{\mathrm{HC}} = \sum_{m=1}^{n} Q_{\mathrm{MMC}m} + Q_{\mathrm{LCC}} \end{cases} \tag{3}$$

P_{MMC} and Q_{MMC} can be expressed as:

$$\begin{cases} P_{\mathrm{MMC}} = \sum_{m=1}^{n} P_{\mathrm{MMC}m} = U_{\mathrm{dcMMC}} I_{\mathrm{dc}} \\ Q_{\mathrm{MMC}} = \sum_{m=1}^{n} Q_{\mathrm{MMC}m} \end{cases} \tag{4}$$

P_{LCC} and Q_{LCC} can be expressed as:

$$\begin{cases} P_{\mathrm{LCC}} = U_{\mathrm{dcLCC}} I_{\mathrm{dc}} \\ Q_{\mathrm{LCC}} = P_{\mathrm{LCC}} \tan\varphi_{\mathrm{r}} = I_{\mathrm{dc}} \sqrt{U_{\mathrm{dcLCC0}}^2 - U_{\mathrm{dcLCC}}^2} \end{cases} \tag{5}$$

U_{dcLCC0} can be expressed as:

$$U_{\mathrm{dcLCC0}} = \frac{3\sqrt{2}}{\pi} N T_{\mathrm{r}} U_{\mathrm{LrN}} U_{\mathrm{Lr,pu}} \tag{6}$$

B. The Control Strategy for HC-HVDC

The control strategy for the HC-HVDC is schematically shown in Fig. 2, where Figs. 2(a) and (b) represent the respective control strategies of the LCC and MMC [26] on the rectifier side, while Fig. 2(c) represents the control of the inverter.

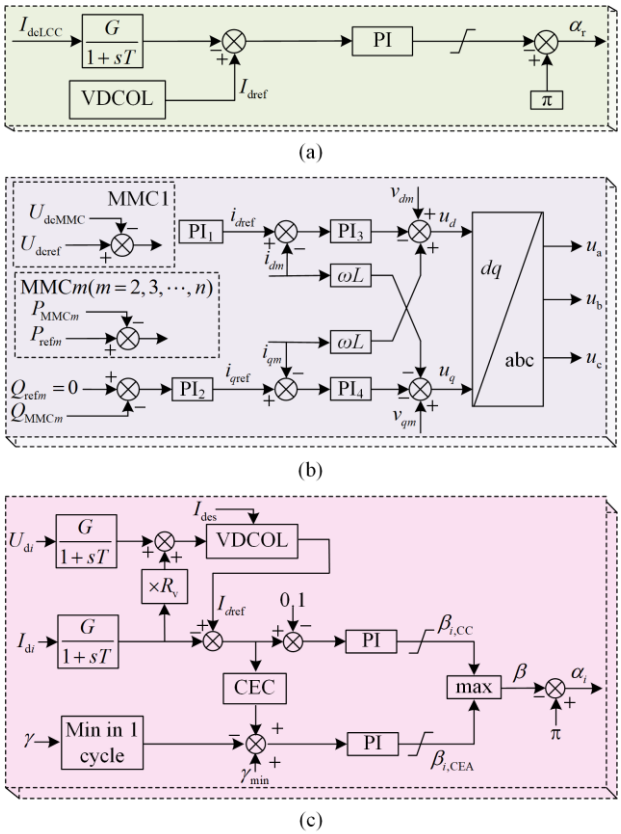

Fig. 2. The control strategies for HC-HVDC. (a) Constant current control of LCC. (b) Vector current control of MMC. (c) LCC inverter control.

In Fig. 2(a), the LCC rectifier adopts constant current control, and in Fig. 2(b), the MMC rectifier adopts current vector control. The outer loop of MMC1 adopts constant DC voltage control, while the remaining MMCs adopt constant active power control to ensure that the total power is evenly distributed among the MMCs. In Fig. 2(c), the LCC inverter adopts constant extinction angle control with additional constant current control.

III. Analysis of Fault Transient Characteristics of the Sending-end AC System

A. Transient Voltage Characteristics and Calculation Method

Figure 3 shows the equivalent circuit of the AC/DC systems after a sending-end AC system fault.

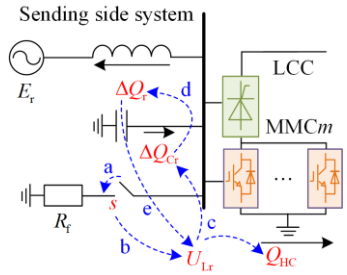

Fig. 3. Equivalent circuit of the AC/DC systems after a sending-end AC system fault.

In Fig. 3, R_{f} is the fault resistance, with different values representing varying fault severities. When a fault occurs in the sending-end AC system, the power balance between the AC and DC hybrid system is disrupted, and the reactive power unbalance of the sending-end system can be expressed as:

$$\Delta Q_{\mathrm{r}} = Q_{\mathrm{acN}} + Q_{\mathrm{Cr}} - \left(Q_{\mathrm{LCC}} + \sum_{m=1}^{n} Q_{\mathrm{MMC}m} \right) \tag{7}$$

The reactive power provided by the AC filter and reactive power compensation devices can be expressed as:

$$Q_{\mathrm{Cr}} = U_{\mathrm{Lr,pu}}^2 Q_{\mathrm{CrN}} \tag{8}$$

The fault propagation path of the sending-end AC system is shown in Fig. 3 from a to e. When a fault occurs in the sending-end AC system (process a), U_{Lr} drops (process b), followed by the drops of U_{dcLCC} and U_{dcMMC}. Since the PI control regulation on the inverter side has a certain lag, it can be obtained from (3) that I_{dc} decreases first. Under the regulation of the inverter control, U_{di} decreases, while I_{dc} briefly rises before dropping along with U_{dr} and U_{di}. The derivative of (5) can be obtained as:

$$\frac{\mathrm{d}Q_{\mathrm{LCC}}}{\mathrm{d}t} = \sqrt{U_{\mathrm{dcLCC0}}^2 - U_{\mathrm{dcLCC}}^2} \frac{\mathrm{d}I_{\mathrm{dc}}}{\mathrm{d}t} - I_{\mathrm{dc}} \frac{U_{\mathrm{dcLCC}} \dfrac{\mathrm{d}U_{\mathrm{dcLCC}}}{\mathrm{d}t}}{\sqrt{U_{\mathrm{dcLCC0}}^2 - U_{\mathrm{dcLCC}}^2}} \tag{9}$$

According to (9), $\mathrm{d}U_{\mathrm{dcLCC}}/\mathrm{d}t<0$, $\mathrm{d}I_{\mathrm{dc}}/\mathrm{d}t<0$, while I_{dc} and U_{dcLCC} are small, and thus, $\mathrm{d}Q_{\mathrm{LCC}}/\mathrm{d}t\mathrm{d}t<0$, and Q_{LCC} is reduced (process c). It can be obtained from (8) that U_{Lr} drop further causes Q_{LCC} to decrease (process c). As Q_{LCC} decreases and the reactive power consumed by the hybrid cascading rectifier (Q_{HC}) changes significantly, the power balance is disrupted (process d), thereby further increasing the degree of transient voltage drop (process e).

According to the above analysis, when a fault occurs in the sending-end AC system, the drop of U_{Lr} consists of two parts: U_{Lrf} caused by the fault at the AC system, and ΔU_{fq} caused by the unbalanced reactive power due to U_{Lr} change. Thus, $U_{\mathrm{Lr,pu}}$ after the fault can be expressed as:

$$U_{\mathrm{Lr,pu}}=\begin{cases}U_{\mathrm{Lr,puf}}+\Delta U_{\mathrm{fq}}, & t\leqslant t_{\mathrm{f}}+t_{\mathrm{dur}}\\ U_{\mathrm{Lr,puN}}+\Delta U_{\mathrm{fq}}, & t>t_{\mathrm{f}}+t_{\mathrm{dur}}\end{cases} \tag{10}$$

$U_{\mathrm{Lr,pu}}$ drops caused by the faults at the sending-end AC system with different fault durations and severities are shown in Fig. 4. The green line in Fig. 4 represents U_{Lrf}, and the red line represents ΔU_{fq}. The four cases are shown in Table I.

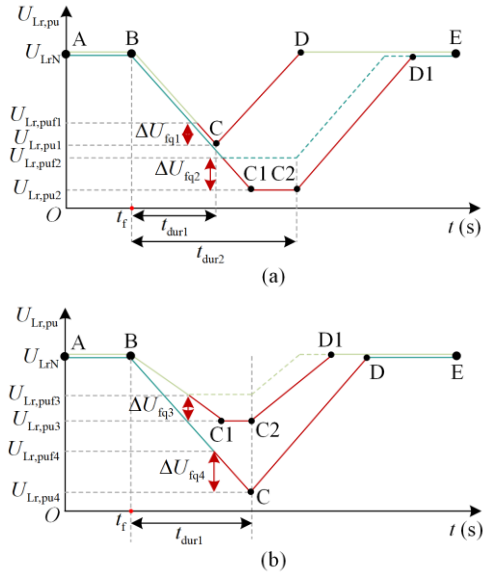

Fig. 4. Transient voltage characteristic diagram. (a) Transient voltage characteristics of different fault durations. (b) Transient voltage characteristics of different fault severity.

TABLE I
DIFFERENT FAILURE SITUATIONS

Case	Fault duration	$U_{\mathrm{Lr,pu}}$	Lines	Figure
1	t_{dur1}	$U_{\mathrm{Lr,pu1}}$	A–B–C–D–E	4(a)
2	t_{dur2}	$U_{\mathrm{Lr,pu2}}$	A–B–C1–C2–D1–E	4(a)
3	t_{dur}	$U_{\mathrm{Lr,pu3}}$	A–B–C1–C2–D1–E	4(b)
4	t_{dur}	$U_{\mathrm{Lr,pu4}}$	A–B–C–D–E	4(b)

Case 1 and case 2 represent the transient voltage characteristics under different fault durations, while case 3 and case 4 represent the transient voltage characteristics under different fault severities.

The transient voltage characteristics caused by the sending-end AC system faults under the same fault severity and different fault durations are compared in Fig. 4(a). In case 1 and case 2, t_{dur1} represents a shorter fault duration while t_{dur2} represents a longer fault duration. The transient voltage variation of case 1 is A–B–C–D–E, and for case 2, it is A–B–C1–C2–D1–E. Under the same fault severity, the transient voltage drop caused by the AC system fault in case 1 is $U_{\mathrm{Lr,puf1}}$ and the voltage change caused by the unbalanced reactive power is ΔU_{fq1}, whereas in case 2, they are $U_{\mathrm{Lr,puf2}}$ and ΔU_{fq2}, respectively. Since the severity of the fault is the same, the voltage drop rates of case 1 and case 2 are identical, showing the same slopes of B–C and B–C1 in Fig. 4(a). However, the fault duration of case 1 is shorter, $U_{\mathrm{Lr,puf1}}<U_{\mathrm{Lr,puf2}}$ and $\Delta U_{\mathrm{fq1}}<\Delta U_{\mathrm{fq2}}$. At the time $t_{\mathrm{f}}+t_{\mathrm{dur1}}$, the converter bus voltage drops to $U_{\mathrm{Lr,pu1}}$, $U_{\mathrm{Lr,pu1}}=U_{\mathrm{Lr,puf1}}+\Delta U_{\mathrm{fq1}}$, which does not reach the minimum transient voltage value under the severity of this fault. The fault duration of case 2 is longer, and at the time $t_{\mathrm{f}}+t_{\mathrm{dur2}}$, $U_{\mathrm{Lr,pu}}$ drops to the minimum value $U_{\mathrm{Lr,pu2}}$, $U_{\mathrm{Lr,pu2}}=U_{\mathrm{Lr,puf2}}+\Delta U_{\mathrm{fq2}}$. If the fault persists for a sufficiently long time, $U_{\mathrm{Lr,pu1}}$ of case 1 will also drop to $U_{\mathrm{Lr,pu2}}$. After the fault clearance, $U_{\mathrm{Lr,pu}}$ is only affected by the unbalanced reactive power.

The transient voltages caused by the sending-end AC system faults under the same fault duration and different fault severities are shown in Fig. 4(b), where case 3 is a minor fault and case 4 is a severe fault. The transient voltage variation in case 3 is A–B–C1–C2–D1–E, and is A–B–C–D–E in case 4. Under the same fault duration, the transient voltage drop caused by the AC system fault in Case 3 is $U_{\mathrm{Lr,puf3}}$ and the voltage change caused by the reactive power change is ΔU_{fq3}, whereas in Case 4 they are $U_{\mathrm{Lr,puf4}}$ and ΔU_{fq4}, respectively. Because of the different fault severities in case 3 and case 4, the voltage drop rates and the slopes of B–C and B–C1 are all different, as shown in Fig. 4(b). Since the fault in case 4 is more severe, the voltage drop of $U_{\mathrm{Lr,pu}}$ is faster, but the fault duration is shorter, while $U_{\mathrm{Lr,pu4}}$ does not reach the minimum voltage drop caused by the AC system fault under this fault severity. Therefore, at the time $t_{\mathrm{f}}+t_{\mathrm{dur}}$, $U_{\mathrm{Lr,pu}}$ eventually drops to $U_{\mathrm{Lr,pu4}}$,

$U_{\mathrm{Lr,pu4}}=U_{\mathrm{Lr,puf4}}+\Delta U_{\mathrm{fq4}}$. However, $U_{\mathrm{Lr,pu4}}$ is not the minimum transient voltage drop in case 4, and if the fault persists for a sufficiently long time, $U_{\mathrm{Lr,pu4}}$ will further drop to its minimum value. The fault severity of case 3 is less so the voltage drop rate is slower. However, at the time $t_{\mathrm{f}}+t_{\mathrm{dur}}$, it has fallen to the minimum value $U_{\mathrm{Lr,pu3}}$, $U_{\mathrm{Lr,pu3}}=U_{\mathrm{Lr,puf3}}+\Delta U_{\mathrm{fq3}}$. After the fault clearance, $U_{\mathrm{Lr,pu}}$ is only affected by the unbalanced reactive power.

According to the above analysis, during the fault in the AC system, $U_{\mathrm{Lr,pu}}$ is the superposition of the voltage drop caused by the fault and the voltage change caused by the unbalanced reactive power. After the fault is cleared, $U_{\mathrm{Lr,pu}}$ is only affected by the voltage variation caused by the unbalanced reactive power.

The relationship between ΔU_{fq} and ΔQ_{r} can be expressed as:

$$\Delta U_{\mathrm{fq}}=\frac{\Delta Q_{\mathrm{r}}}{S_{\mathrm{cr}}} \tag{11}$$

The AC system strength is usually measured by the short circuit ratio, which can be expressed as:

$$\zeta_{\mathrm{SCR}}=\frac{S_{\mathrm{cr}}}{P_{\mathrm{dN}}} \tag{12}$$

Substituting (7), (8), (11), (12) into (10), $U_{\mathrm{Lr,pu}}$ can be expressed as:

$$U_{\mathrm{Lr,pu}}=\begin{cases}U_{\mathrm{Lr,puf}}+\dfrac{Q_{\mathrm{acN}}+U_{\mathrm{Lr,pu}}^2Q_{\mathrm{CrN}}-\left(Q_{\mathrm{LCC}}+\sum_{m=1}^{n}Q_{\mathrm{MMC}m}\right)}{\zeta_{\mathrm{SCR}}P_{\mathrm{dN}}}, & t\leqslant t_{\mathrm{f}}+t_{\mathrm{dur}}\\ U_{\mathrm{Lr,puN}}+\dfrac{Q_{\mathrm{acN}}+U_{\mathrm{Lr,pu}}^2Q_{\mathrm{CrN}}-\left(Q_{\mathrm{LCC}}+\sum_{m=1}^{n}Q_{\mathrm{MMC}m}\right)}{\zeta_{\mathrm{SCR}}P_{\mathrm{dN}}}, & t>t_{\mathrm{f}}+t_{\mathrm{dur}}\end{cases} \tag{13}$$

$U_{\mathrm{Lr,pu}}$ for HC-HVDC can be calculated as:

$$U_{\mathrm{Lr,pu}}=\begin{cases}\dfrac{\zeta_{\mathrm{SCR}}P_{\mathrm{dN}}}{2Q_{\mathrm{CrN}}}-\sqrt{\left(\dfrac{\zeta_{\mathrm{SCR}}P_{\mathrm{dN}}}{2Q_{\mathrm{CrN}}}\right)^2-\dfrac{\zeta_{\mathrm{SCR}}P_{\mathrm{dN}}U_{\mathrm{Lr,puf}}}{Q_{\mathrm{CrN}}}-\dfrac{Q_{\mathrm{acN}}}{Q_{\mathrm{CrN}}}+\dfrac{\left(Q_{\mathrm{LCC}}+\sum_{m=1}^{n}Q_{\mathrm{MMC}m}\right)}{Q_{\mathrm{CrN}}}}, & t\leqslant t_{\mathrm{f}}+t_{\mathrm{dur}}\\ \dfrac{\zeta_{\mathrm{SCR}}P_{\mathrm{dN}}}{2Q_{\mathrm{CrN}}}-\sqrt{\left(\dfrac{\zeta_{\mathrm{SCR}}P_{\mathrm{dN}}}{2Q_{\mathrm{CrN}}}\right)^2-\dfrac{\zeta_{\mathrm{SCR}}P_{\mathrm{dN}}U_{\mathrm{Lr,puN}}}{Q_{\mathrm{CrN}}}-\dfrac{Q_{\mathrm{acN}}}{Q_{\mathrm{CrN}}}+\dfrac{\left(Q_{\mathrm{LCC}}+\sum_{m=1}^{n}Q_{\mathrm{MMC}m}\right)}{Q_{\mathrm{CrN}}}}, & t>t_{\mathrm{f}}+t_{\mathrm{dur}}\end{cases} \tag{14}$$

B. Influence Factors of Transient Voltage

According to (14), during a fault in the sending-end AC system, the variables affecting the transient overvoltage are mainly divided into three categories. The first one is the fault severity, which determines $U_{\mathrm{Lr,puf}}$, and is affected by the fault itself. The second one is the static factors that are not affected by transient DC current and DC voltage, including ζ_{SCR} and Q_{CrN}. The third one is the dynamic influence factors affected by transient DC current and DC voltage, including Q_{LCC} and Q_{MMC}. According to the classification of the influencing factors, the commutation bus voltage support schemes can be divided into two categories. The first category is to regulate the operation mode of the system and provide enhanced reactive power support for the AC system during the fault, and the second category is to adjust the response characteristics of the converter during the fault to reduce the resultant unbalanced reactive power, as shown in Fig. 5.

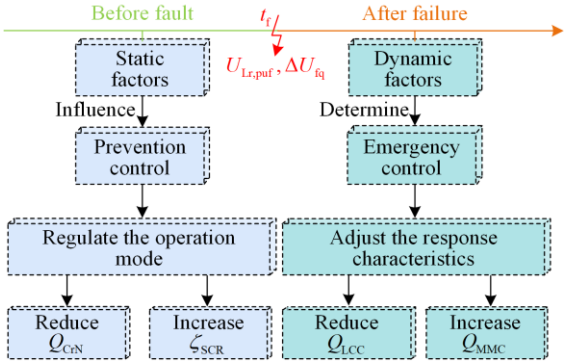

Fig. 5. Influence factors of transient voltage.

Substituting (8) into (13), $U_{\mathrm{Lr,pu}}$ can be calculated as:

$$U_{\mathrm{Lr,pu}}=\begin{cases}U_{\mathrm{Lr,puf}}+\dfrac{Q_{\mathrm{acN}}+Q_{\mathrm{Cr}}-\left(Q_{\mathrm{LCC}}+\sum_{m=1}^{n}Q_{\mathrm{MMC}m}\right)}{\zeta_{\mathrm{SCR}}P_{\mathrm{dN}}}, & t\leqslant t_{\mathrm{f}}+t_{\mathrm{dur}}\\ U_{\mathrm{Lr,puN}}+\dfrac{Q_{\mathrm{acN}}+Q_{\mathrm{Cr}}-\left(Q_{\mathrm{LCC}}+\sum_{m=1}^{n}Q_{\mathrm{MMC}m}\right)}{\zeta_{\mathrm{SCR}}P_{\mathrm{dN}}}, & t>t_{\mathrm{f}}+t_{\mathrm{dur}}\end{cases} \tag{15}$$

During the fault and for a given degree of fault severity, $U_{\mathrm{Lr,puf}}$ is a fixed value, while the voltage change caused by the unbalanced reactive power affects the transient voltage. It can be known from (15) that Q_{Cr} is positively correlated with $U_{\mathrm{Lr,pu}}$, and thus, $U_{\mathrm{Lr,pu}}$ can be supported by improving the reactive power support during the fault. When $t>t_{\mathrm{f}}+t_{\mathrm{dur}}$, the fault recovery speed can be accelerated by increasing the reactive power support during

the recovery period, since the AC voltage is only affected by the unbalanced reactive power.

When $P_{dN}=4000$ MW, $Q_{acN}=0$ Mvar, and $Q_{CrN}=1250$ Mvar, the effects of different $U_{Lr,puf}$ and ζ_{SCR} on the system are shown in Fig. 6.

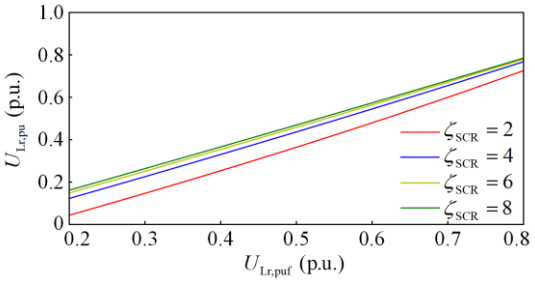

Fig. 6. Diagram of $U_{Lr,puf}$ and ζ_{SCR} influence on transient voltage.

In (15), ζ_{SCR} mainly affects the voltage variation caused by unbalanced reactive power, and is negatively correlated with $U_{Lr,pu}$. The smaller ζ_{SCR}, the greater impact of unbalanced reactive power fluctuation on transient voltage, indicating that small changes in converter reactive power consumption can have a large impact on transient voltage. It can be seen from Fig. 6 that, the increase of ζ_{SCR} leads to lower transient voltage drop under the same fault severity (same $U_{Lr,puf}$).

When $\zeta_{SCR}=2.5$, $P_{dN}=4000$ MW, $Q_{acN}=0$ Mvar, and $Q_{CrN}=1250$ Mvar, the relationships among $U_{Lr,pu}$, $U_{Lr,puf}$, and Q_{LCC} are shown in Fig. 7, with $\sum_{m=1}^{n}Q_{MMCm}$ being 0 Mvar, 500 Mvar, and −500 Mvar, respectively.

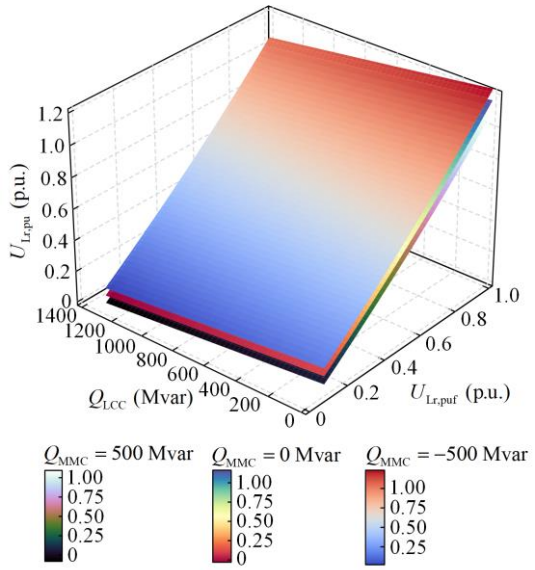

Fig. 7. Relationship among $U_{Lr,pu}$, $U_{Lr,puf}$, and Q_{LCC}.

It can be seen from Fig. 7 that, when $(Q_{LCC}+Q_{MMC})$ remains constant, the increase in fault severity results in reduced $U_{Lr,puf}$ and $U_{Lr,pu}$ nonlinearity. For a given degree of fault severity, $U_{Lr,puf}$ is fixed and the increase of $(Q_{LCC}+Q_{MMC})$ further reduces $U_{Lr,pu}$. In severe cases, this may cause the new energy units to trip, turning a single fault into a cascading fault.

IV. Voltage Support Strategy of Sending-End AC System

A. Analysis of Transient Voltage Characteristics Considering the Reactive Power Support of MMC

MMC has the ability to support reactive power. By jointly using the MMC and reactive power compensation devices to support the sending-end system, reactive power can be provided to better support $U_{Lr,pu}$ during the fault in the sending-end AC system. The reactive power provided by the AC filter and reactive power compensation devices is Q_{Cr}, whereas it is Q_{CrN} under the rated voltage, while their relationship is shown in (8). It is assumed that the reactive power provided by the MMC to the AC system at the sending-end is Q_{MMC}. Under such conditions, the reactive power provided by the AC filter and reactive power compensation devices is now expressed as Q'_{Cr} while its rated value is Q'_{CrN}, and the two can be expressed, similar to (8), as:

$$Q'_{Cr}=U^2_{Lr,pu}Q'_{CrN} \tag{16}$$

In steady-state operation, Q_{CrN} is satisfied with Q'_{CrN}:

$$Q_{CrN}=Q'_{CrN}+Q_{MMC} \tag{17}$$

When $U_{Lr,pu}$ changes, to determine the magnitude of Q_{Cr} and Q'_{Cr}, a function of $f(U_{Lr,pu})$ is given as:

$$\begin{aligned} f(U_{Lr,pu})&=Q_{Cr}-\left(Q'_{Cr}+Q_{MMC}\right)= \\ &U^2_{Lr,pu}Q_{CrN}-\left(U^2_{Lr,pu}Q'_{CrN}+Q_{MMC}\right) \end{aligned} \tag{18}$$

Substituting (17) into (18), when the $U_{Lr,pu}$ changes, $f(U_{Lr,pu})$ can be expressed as:

$$f(U_{Lr,pu})=U^2_{Lr,pu}\left(Q'_{CrN}+Q_{MMC}\right)-\left(U^2_{Lr,pu}Q'_{CrN}+Q_{MMC}\right) \tag{19}$$

The image of function $f(U_{Lr,pu})$ is shown in Fig. 8.

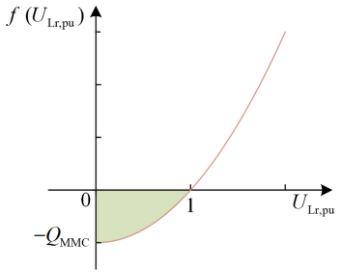

Fig. 8. The function image of $f(U_{Lr,pu})$.

When a fault occurs in the sending-end AC system, $U_{\mathrm{Lr,pu}}$ drops. As shown in the green area in Fig. 8, when $U_{\mathrm{Lr,pu}}$ is less than 1, $f(U_{\mathrm{Lr,pu}})$ is always less than 0, i.e., $(Q'_{\mathrm{Cr}}+Q_{\mathrm{MMC}})$ is always greater than Q_{Cr}. Therefore, if the MMC and the reactive power compensation devices are used to provide reactive power for the AC system in steady state, better reactive power support can be provided for the AC system during the fault, and the voltage drop is reduced.

Because the MMC uses constant DC voltage (constant active power)/constant reactive power control, to maximize active power transmission, the MMC reactive power order is 0 in steady state, $Q_{\mathrm{ref}m}=0$ Mvar. However, the rated capacity S_{MMC} of the MMC is often larger than its rated active power, and the maximum MMC reactive power regulation capability $Q_{\mathrm{MMC}m}$ in steady-state operation can be expressed as:

$$Q_{\mathrm{MMC}m}=\sqrt{S_{\mathrm{MMC}}^2-P_{\mathrm{MMC}m}^2} \tag{20}$$

The total reactive power provided by all the MMCs can be calculated as:

$$Q_{\mathrm{MMC}}=Q_{\mathrm{MMC1}}+\sum_{m=2}^{n}Q_{\mathrm{MMC}m} \tag{21}$$

When the reactive power support of the MMCs is considered, the reactive power balance in the stable operation of the system can be expressed as:

$$Q_{\mathrm{LCC}}=Q_{\mathrm{ac}}+Q'_{\mathrm{Cr}}+\sum_{m=1}^{n}Q_{\mathrm{MMC}m} \tag{22}$$

After a fault occurs in the sending-end AC system, the unbalanced reactive power can be expressed as:

$$\Delta Q_{\mathrm{r}}=Q_{\mathrm{acN}}+Q'_{\mathrm{Cr}}+\sum_{m=1}^{n}Q_{\mathrm{MMC}m}-Q_{\mathrm{LCC}} \tag{23}$$

Substituting (23) and (16) into (10), when $t\leqslant t_{\mathrm{f}}+t_{\mathrm{dur}}$, $U'_{\mathrm{Lr,pu}}$ can be expressed as:

$$Q_{\mathrm{acN}}+U_{\mathrm{Lr,pu}}^2Q'_{\mathrm{CrN}}+U'_{\mathrm{Lr,pu}}=U_{\mathrm{Lr,puf}}+\frac{\sum_{m=1}^{n}Q_{\mathrm{MMC}m}-Q_{\mathrm{LCC}}}{\zeta_{\mathrm{SCR}}P_{\mathrm{dN}}} \tag{24}$$

$U'_{\mathrm{Lr,pu}}$ can be calculated as:

$$U'_{\mathrm{Lr,pu}}=\frac{\zeta_{\mathrm{SCR}}P_{\mathrm{dN}}}{2Q'_{\mathrm{CrN}}}-\sqrt{\left(\frac{\zeta_{\mathrm{SCR}}P_{\mathrm{dN}}}{2Q'_{\mathrm{CrN}}}\right)^2-\frac{\zeta_{\mathrm{SCR}}P_{\mathrm{dN}}U_{\mathrm{Lr,puf}}}{Q'_{\mathrm{CrN}}}-\frac{Q_{\mathrm{acN}}}{Q'_{\mathrm{CrN}}}-\frac{\sum_{m=1}^{n}Q_{\mathrm{MMC}m}}{Q'_{\mathrm{CrN}}}+\frac{Q_{\mathrm{LCC}}}{Q'_{\mathrm{CrN}}}} \tag{25}$$

According to (25) and (14), for $\zeta_{\mathrm{SCR}}=2.5$, $P_{\mathrm{dN}}=4000$ MW, and $Q_{\mathrm{acN}}=0$ Mvar, the relationship between $U'_{\mathrm{Lr,pu}}/U_{\mathrm{Lr,pu}}$ and $U_{\mathrm{Lr,puf}}$ is shown in Fig. 9 for different Q'_{Cr}.

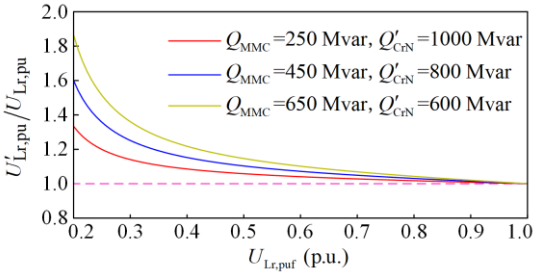

Fig. 9. The relationship of $U_{\mathrm{Lr,pu}}$ and $U_{\mathrm{Lr,puf}}$.

It can be seen from Fig. 9 that, during the fault, $U'_{\mathrm{Lr,pu}}/U_{\mathrm{Lr,pu}}$ is always greater than 1 at any fault severity. It can be concluded that the transient voltage drop under the MMC reactive power support is less severe. Smaller $U_{\mathrm{Lr,puf}}$ leads to larger ratio of $U'_{\mathrm{Lr,pu}}/U_{\mathrm{Lr,pu}}$, indicating more significant supporting effect of the MMC on the system during the fault. This is because the more severe the fault is, the greater the voltage changes as the result of the fault, resulting in less reactive power provided by the AC filter and reactive power compensation devices, and a more significant voltage change by the unbalanced reactive power. According to the three sets of curves, larger MMC reactive power support leads to smaller Q'_{Cr}, larger ratio of $U'_{\mathrm{Lr,pu}}/U_{\mathrm{Lr,pu}}$, and lower the voltage drop during the fault.

B. The Influence of Q_{LCC} on Transient Voltage

Q_{LCC} is a dynamic factor affecting the transient voltage, and to further clarify its influence, the relationships between Q_{LCC} and $U_{\mathrm{Lr,pu}}$ under different fault severities according to (25) and (14) are shown in Fig. 10, with $\zeta_{\mathrm{SCR}}=2.5$, $P_{\mathrm{dN}}=4000$ MW, $Q_{\mathrm{acN}}=0$ Mvar, $Q_{\mathrm{CrN}}=1250$ Mvar, and $\sum_{m=1}^{n}Q_{\mathrm{MMC}m}=0$ MVar.

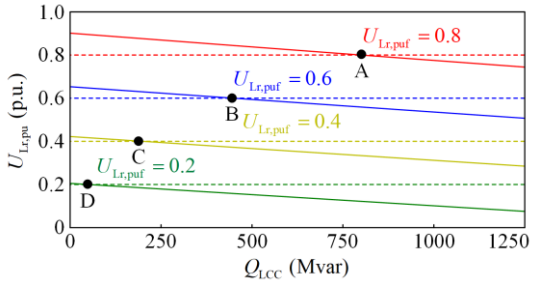

Fig. 10. The effect of Q_{LCC} and $U_{\mathrm{Lr,puf}}$ on transient voltage.

It can be obtained from Fig. 10, the $U_{\mathrm{Lr,pu}}$ and $U_{\mathrm{Lr,puf}}$ curves have four intersection points (A, B, C, D) where $U_{\mathrm{Lr,pu}}=U_{\mathrm{Lr,puf}}$ and the unbalanced reactive power is 0, i.e., $\Delta Q_{\mathrm{r}}=0$ Mvar. The intersection point is defined as the reactive balance point, and the LCC reactive power

consumption at this point is the critical reactive power consumption Q_{LCC}^{*}, which indicates that Q_{LCC} is equal to the reactive power provided by the AC filter and reactive power compensation devices. When $Q_{\mathrm{LCC}} > Q_{\mathrm{LCC}}^{*}$, the reactive power consumption of the rectifier will cause $\Delta Q_{\mathrm{r}} < 0$, leading to further voltage drop and worsening of the fault. When $Q_{\mathrm{LCC}} < Q_{\mathrm{LCC}}^{*}$, the reactive power consumption of the rectifier decreases, causing $\Delta Q_{\mathrm{r}} > 0$, which enhances the reactive power support to the AC system and does not aggravate the fault. With the increase of the fault severity, the DC transmission power decreases, and the DC current and DC voltage also decrease with the drop of $U_{\mathrm{Lr,pu}}$. The reactive balance point will move to the left, as shown in points A and D, the adjustable range of Q_{LCC} is reduced, and the reactive power support ability of the AC system is further weakened. Q_{LCC}^{*} can be expressed as:

$$Q_{\mathrm{LCC}}^{*} = Q_{\mathrm{acN}} + U_{\mathrm{Lr,puf}}^{2} Q_{\mathrm{CrN}} - \sum_{m=1}^{n} Q_{\mathrm{MMC}m} \tag{26}$$

Furthermore, when $\sum_{m=1}^{n} Q_{\mathrm{MMC}m}$=450 MVar and $U_{\mathrm{Lr,puf}} = 0.5$, the relationship between Q_{LCC} and $U_{\mathrm{Lr,pu}}$ can be obtained as shown in Fig. 11.

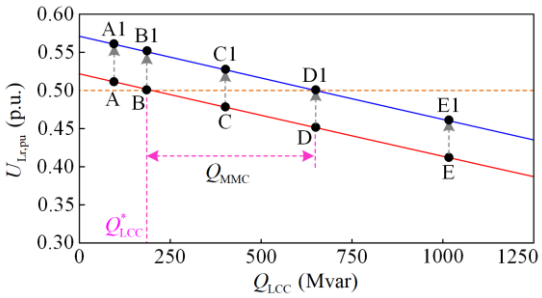

Fig. 11. The influence of Q_{LCC} and $U_{\mathrm{Lr,puf}}$ on transient voltage after MMC reactive power support is considered.

In Fig. 11, the pink line is the reactive power support provided by the MMC, Q_{LCC}^{*} which considers the reactive power support of the MMC, can be expressed as:

$$Q_{\mathrm{LCC}}^{*} = Q_{\mathrm{acN}} + U_{\mathrm{Lr,puf}}^{2} Q'_{\mathrm{CrN}} \tag{27}$$

When Q_{LCC} is at point A in Fig. 11, $Q_{\mathrm{LCC}} < Q_{\mathrm{LCC}}^{*}$, the LCC does not cause further drop of $U_{\mathrm{Lr,pu}}$ and can support the AC voltage. Considering the reactive power support provided by the MMC, the LCC and MMC jointly support the sending-end AC system and reduce the transient voltage drop, $U_{\mathrm{Lr,pu}} > U_{\mathrm{Lr,puf}}$, so the actual operating point moves from points A to A1. When Q_{LCC} is at point B in Fig. 11, $Q_{\mathrm{LCC}} = Q_{\mathrm{LCC}}^{*}$, the LCC will neither support nor deteriorate the transient voltage. Under such conditions, the MMC still supports the AC system and reduces the transient voltage drop, $U_{\mathrm{Lr,pu}} > U_{\mathrm{Lr,puf}}$, so the actual operating point moves from points B to B1. When Q_{LCC} is at point C in Fig. 11, $Q_{\mathrm{LCC}} > Q_{\mathrm{LCC}}^{*}$, the LCC deteriorates the transient voltage. Considering the reactive power support provided by the MMC, as $Q_{\mathrm{LCC}} - Q_{\mathrm{LCC}}^{*} < Q_{\mathrm{MMC}}$, while the LCC weakens the reactive power supporting capability of the MMC, the MMC's reactive power support remains effective. $U_{\mathrm{Lr,pu}} > U_{\mathrm{Lr,puf}}$, the actual operating point moves from points C to C1. When Q_{LCC} is at point D in Fig. 11, $Q_{\mathrm{LCC}} > Q_{\mathrm{LCC}}^{*}$, the LCC deteriorates the transient voltage. Considering the reactive power support provided by the MMC, as $Q_{\mathrm{LCC}} - Q_{\mathrm{LCC}}^{*} = Q_{\mathrm{MMC}}$, the LCC offsets the reactive power support of MMC, thereby making the reactive power support of MMC ineffective. $U_{\mathrm{Lr,pu}} = U_{\mathrm{Lr,puf}}$, the actual operating point moves from points D to D1. When Q_{LCC} is at point E in Fig. 11, $Q_{\mathrm{LCC}} > Q_{\mathrm{LCC}}^{*}$, the LCC deteriorates the transient voltage. Considering the reactive power support provided by the MMC, as $Q_{\mathrm{LCC}} - Q_{\mathrm{LCC}}^{*} > Q_{\mathrm{MMC}}$, the reactive power support provided by the MMC cannot meet the reactive power consumption of the LCC, causing the transient voltage to decrease further. $U_{\mathrm{Lr,pu}} < U_{\mathrm{Lr,puf}}$, and the actual operating point moves from points E to E1. However, the transient voltage at E1 is still larger than that at E. Therefore, the reactive power support provided by the MMC can avoid or reduce the adverse effect of the LCC on transient voltage.

C. Transient Voltage Support Strategy

According to the analysis in Fig. 11 and Section IV.B, the transient voltage support strategy of the sending-end can be divided into two parts. In steady state, according to (22), the MMC is used to replace part of the reactive power compensation devices to reduce the reactive power compensation capacity of the rectifier station. The MMC and reactive power compensation devices jointly support the AC system of the sending-end. In the transient state, it is necessary to determine the reactive power balance point according to the fault severity to ensure that Q_{LCC} does not exceed Q_{LCC}^{*}, such that the reactive power consumption of the MMC can be maximized.

In order to measure the fault severity, $U_{\mathrm{Lr,puf}}$ can be calculated as:

$$U_{\mathrm{Lr,puf}} = U'_{\mathrm{Lr,pu}} - \frac{Q_{\mathrm{acN}} + U'^{2}_{\mathrm{Lr,pu}} Q'_{\mathrm{CrN}} + \sum_{m=1}^{n} Q_{\mathrm{MMC}m} - Q_{\mathrm{LCC}}}{\zeta_{\mathrm{SCR}} P_{\mathrm{dN}}} \tag{28}$$

Substituting (28) into (27), Q_{LCC}^{*} can be calculated as:

$$Q^*_{\mathrm{LCC}} = I^*_{\mathrm{dc}}\sqrt{U^2_{\mathrm{dcLCC0}} - U^2_{\mathrm{dcLCC}}} = Q_{\mathrm{acN}} + U'^2_{\mathrm{Lr,puf}}Q'_{\mathrm{CrN}} \quad (29)$$

I^*_{dc} can be calculated as:

$$I^*_{\mathrm{dc}} = \frac{Q^*_{\mathrm{LCC}}}{\sqrt{U^2_{\mathrm{dcLCC0}} - U^2_{\mathrm{dcLCC}}}} \quad (30)$$

According to (30), I^*_{dcref} can be calculated as:

$$I^*_{\mathrm{dcref}} = \frac{I^*_{\mathrm{dc}}}{I_{\mathrm{dcN}}} \quad (31)$$

When $Q_{\mathrm{LCC}} > Q^*_{\mathrm{LCC}}$, the DC system adopts (31) as the DC current order to ensure that the reactive power consumed by the LCC does not deteriorate the transient voltage under severe faults. This also mitigates the weakening effect of the LCC to MMC's reactive power support and maximize the MMC's contribution to system reactive power support.

According to (25), (30), and (31), an MMC and LCC cooperation support strategy for the sending-end AC system is proposed, as shown in Fig. 12.

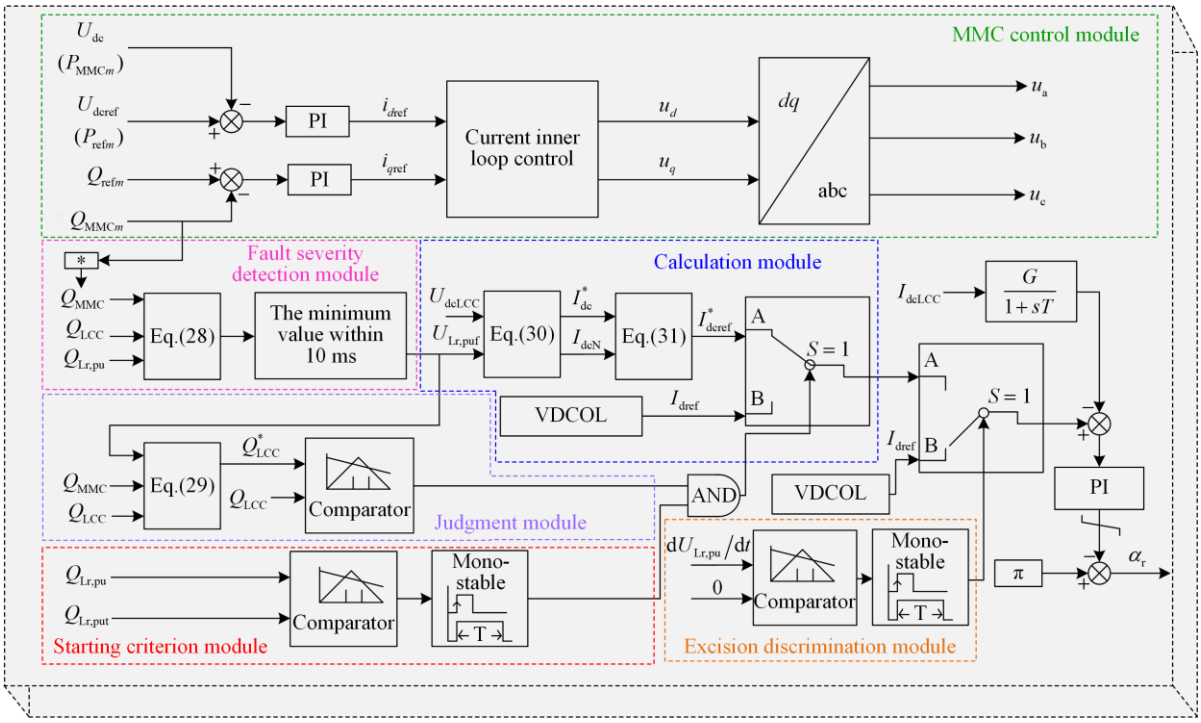

Fig. 12. Cooperative transient voltage support strategy for multiple converters.

In Fig. 12, the proposed strategy mainly includes an MMC control module and an LCC control module. The LCC control module includes a fault severity detection module, a calculation module, a starting criterion module, a judgment module, and an excision discrimination module.

In steady state, the MMC control module sets the reactive power order of the MMC to a none-zero Q_{refm}, so that the MMC and the reactive power compensation devices jointly support the sending-end AC system.

When a fault occurs in the sending-end AC system, the LCC starting the criterion module determines whether the starting condition of the proposed strategy is satisfied by comparing the pre-set voltage threshold $U_{\mathrm{Lr,put}}$ with the measured $U_{\mathrm{Lr,pu}}$. At the same time, the sensitivity of fault identification can be adjusted by adjusting $U_{\mathrm{Lr,put}}$.

Fault severity detection uses Q_{LCC}, Q_{MMC}, and $U_{\mathrm{Lr,pu}}$ to calculate $U_{\mathrm{Lr,puf}}$ according to (28) to determine the severity of the fault.

Then, the judgment module calculates Q^*_{LCC} according to Q_{LCC}, Q_{MMC}, and $U_{\mathrm{Lr,pu}}$, determines the power balance point, and judges the size of the two according to the measured Q_{LCC} to further determine whether the LCC will weaken MMC's reactive power support.

The calculation module uses $U_{\mathrm{Lr,puf}}$ calculated by the fault severity detection module and the measured U_{dcLCC} to calculate I^*_{dcref}, according to (30) and (31). When both the starting criterion and judgment modules are satisfied, I^*_{dcref} is output to the rectifier side LCC constant current controller. Otherwise, VDCOL control is maintained.

Finally, the judgment module calculates $\mathrm{d}U_{\mathrm{Lr,pu}}/\mathrm{d}t$ and compares it with 0. When $U_{\mathrm{Lr,pu}}$ begins to rise, the proposed strategy is removed and the VDCOL control is restored.

V. Case Studies

The PSCAD/EMTDC platform is used to verify the correctness of the theory and the effectiveness of the proposed strategy. Based on the CIGRE HVDC standard test system, a HC-HVDC as shown in Fig. 1 is developed. The parameters of the HC-HVDC are shown in Table II. Cases A, B, C, D, E and F are simulated to illustrate the transient voltage characteristics and transient voltage support effects under different fault severities, types, and durations, as listed in Table III.

TABLE II
Parameters of the Hybrid Cascaded HVDC

System parameter	Value
Rated capacity (MW)	4000
DC voltage (kV)	800
DC current (kA)	5
Extinction angle (°)	17
Number of MMC	3
DC current of each MMC (kA)	1.667
Number of bridge arm sub-modules per phase	200
Sub-module capacitance voltage (kV)	2

TABLE III
Overview of the Cases

Case	Fault type	R_f/L_f	t_{dur} (s)	Figure
A	TPG	150 Ω	0.2	13(a)
B	TPG	10 Ω	0.2	13(b)
C	LLG	10 Ω	0.2	13(c)
D	TPG	10 Ω	0.1	13(d)
E	TPG	0.1 H	0.2	13(e)
F	TPG	0.7 H	0.2	13(f)

$Q_{MMC}=0$ Mvar, $Q_{CrN}=1250$ Mvar, $Q_{MMC}=400$ Mvar, $Q_{CrN}=850$ Mvar, $Q_{MMC}=600$ Mvar, and $Q_{CrN}=650$ Mvar are used as an example for simulation. In this paper, a negative value of Q_{MMC} indicates that the MMC provides reactive power to the network.

Figure 13 depicts the simulation results for the different cases shown in Table III. Cases A and B have the same fault type (TPG) and fault duration ($t_{dur}=0.2$ s), but different fault severities ($R_f=150\,\Omega$ and $R_f=10\,\Omega$, respectively), representing a minor fault and a severe fault. Cases B and C have the same fault severity ($R_f=10\,\Omega$) and fault duration ($t_{dur}=0.2$ s), but different fault types of TPG and LLG, representing symmetric and asymmetric faults. Cases B and D have the same fault severity ($R_f=10\,\Omega$) and fault type (TPG), but different fault durations of 0.2 s and 0.1 s. Cases E and F have the same fault type (TPG) and fault duration ($t_{dur}=0.2$ s), but different fault inductances of 0.1 H and 0.7 H, representing different fault locations.

It can be seen from (A1)–(D1) in Fig. 13 that, with the increase of Q_{MMC} at steady state, the steady-state Q_{Cr} decreases, while the sum of Q_{MMC} and Q_{Cr} remains unchanged. After the fault occurs in the sending-end AC system, the larger the Q_{MMC}, the smaller the change of Q_{Cr} and the Q_{CrN}. From (8), it can be seen that the smaller the Q_{CrN}, the smaller the Q_{Cr} change in the system under the same voltage change. In addition, as larger Q_{MMC} provides stronger support to the sending-end AC system by the MMC after the fault, the voltage change becomes smaller. It can be seen from (A1) and (B1) that when a less severe fault occurs in the sending-end AC system, the voltage drop is relatively small, and the reactive power compensation devices also have high reactive power support capability. It can be seen from (B1) and (C1) that when a severe fault occurred in the sending-end AC system, the voltage drop is significant, and Q_{Cr} cannot support the sending end AC system. It can be seen from (B1) and (D1) that if the fault duration of the system is short and the voltage does not drop to the minimum value, the support of the reactive power compensation devices to the sending-end AC system after the fault increases. It can be seen from (E1) and (F1) that, the larger the fault inductance, the farther the distance between the fault point and the converter bus. In addition, the less severe the fault is, the more the support is provided by the reactive power compensation devices to the AC system after the fault.

It can be seen from (A2)–(D2) in Fig. 13 that after the system failure, the fluctuation of Q_{MMC} is small during the fault. Therefore, the increase of Q_{MMC} provides enhanced support on $U_{Lr,pu}$ during the fault. According to (A2)–(B2), when the system fault is less severe, the fluctuation of Q_{MMC} is smaller and the support on $U_{Lr,pu}$ is stronger during the fault. It can be seen from (E2)–(F2) that the farther the fault point is from the converter bus, the smaller the fluctuation of Q_{MMC} is, and the more reactive power support of the MMC to the AC system is during the transient period.

It can be seen from (A3)–(D3) in Fig. 13 that, the transient voltages under different fault severities, types, durations and locations are increased after adopting the proposed strategy in this paper. According to the simulation results of Q_{Cr} and Q_{MMC}, it can be concluded that the deterioration of transient voltage caused by unbalanced reactive power can be alleviated with the reactive power support of the MMC and the reactive power regulation function of the LCC, effectively preventing further transient voltage drop during the fault. The minimum transient voltages of different cases are shown in Table IV. According to Table IV and (A3)–(F3) in Fig. 13, it can be obtained that the more severe the fault occurs in the sending-end AC system, the better the voltage support effect is. Under the same fault severity, the voltage support effect is better when

the symmetrical fault occurs in the sending-end AC system. Under the same fault type and severity, the closer the fault location is, the better the voltage support effect is. In addition, the larger the reactive power support provided by the MMC, the better the transient voltage improvement effect.

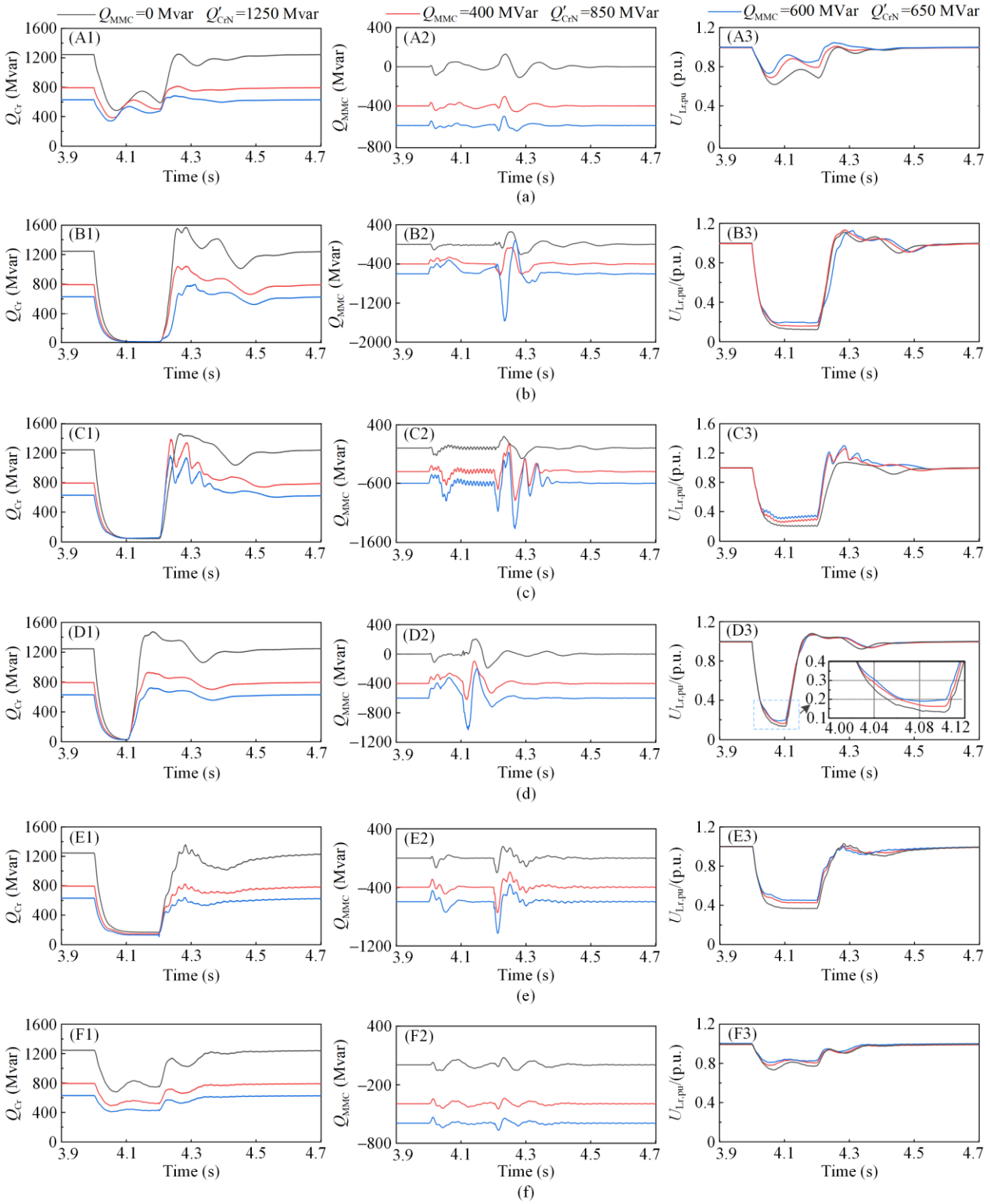

Fig. 13. Simulation results of transient voltage support strategies under different cases. (a) Case A: (A1)–(A3), TPG fault with $R_f = 150\,\Omega$ and $t_{dur} = 0.2$ s. (b) Case B: (B1)–(B3), TPG fault with $R_f = 10\,\Omega$ and $t_{dur} = 0.2$ s. (c) Case C: (C1)–(C3), LLG fault with $R_f = 10\,\Omega$ and $t_{dur} = 0.2$ s. (d) Case D: (D1)–(D3), TPG fault with $R_f = 10\,\Omega$ and $t_{dur} = 0.1$ s. (e) Case E: (E1)–(E3), TPG fault with $L_f = 0.1$ H and $t_{dur} = 0.2$ s. (f) Case F: (F1)–(F3), TPG fault with $L_f = 0.7$ H and $t_{dur} = 0.2$ s.

TABLE IV
COMPARISON OF MINIMUM TRANSIENT VOLTAGE

Case	Transient voltage (p.u.)				
	Q_{MMC} : 0 Mvar	Q_{MMC} : 400 Mvar	Increase ratio (%)	Q_{MMC} : 600 Mvar	Increase ratio (%)
A	0.62	0.69	11.30	0.73	18.37
B	0.12	0.16	31.41	0.19	58.00
C	0.20	0.25	26.26	0.30	50.73
D	0.13	0.16	23.41	0.19	43.93
E	0.36	0.42	15.44	0.45	23.13
F	0.73	0.78	6.34	0.80	9.55

The strategy proposed in this paper is removed during the recovery process, so the switching of the DC current order will not deteriorate the fault recovery process. Therefore, after fault clearance, the times for the voltage to recover to the rated value in the improved and original systems are largely the same. The effectiveness of the proposed strategy is verified by the simulation results under different fault severities, types, durations, and locations.

VI. DISCUSSION

For the sending-end HC-HVDC, the capacities of the LCC and MMC and the switching time of the coordinated control are the key factors affecting the voltage support of the sending-end AC system.

As shown in Fig. 13, following an AC system fault, it is necessary to adjust the LCC's reactive power consumption, so as to maximize the MMC's reactive power support effect. However, the adjustment time of the DC current will affect the voltage recovery after fault clearing. The proposed strategy must be removed when $U_{\mathrm{Lr,pu}}$ rises. In the event of a severe fault in the sending-end AC system, it can be seen from Fig. 11 that the critical reactive power consumption of the LCC is small. After the fault is cleared, due to the rapid rise of $U_{\mathrm{Lr,pu}}$, Q_{Cr} increases rapidly and if the reactive power consumed by the LCC remains low, there may be a risk of transient overvoltage in the recovery stage.

In addition, the active power ratio of the LCC to MMC is 1:1 in this paper. The proportion of the LCC and MMC active power also affects the effectiveness of the proposed strategy. For an MMC with a given capacity, the more active power it transmits, the less reactive power support it can provide, reducing its effectiveness in supporting the transient voltage. Using an MMC with larger capacity will increase the system's construction cost.

VII. CONCLUSION

This paper aims at the transient voltage caused by sending-end AC system faults in a HC-HVDC system. A transient voltage calculation method considering fault duration and severity is established, and a transient voltage support strategy based on coordinated control of LCC and MMC is proposed. The conclusions are summarized as follows.

1) There is a strong coupling between the sending-end AC system and HC-HVDC after faults in the sending-end AC system. The fault severity and duration, and the reactive power compensation devices of the converter are the key factors affecting the transient voltage characteristics.

2) During a fault, the reactive power consumption of the LCC and the change of reactive power provided by the reactive power compensation devices cause unbalanced reactive power between the AC/DC systems, increasing the risk of deteriorating the transient voltage.

3) Compared to methods that only use reactive power compensation devices, the proposed scheme combines the MMC and reactive power compensation devices to provides stronger reactive power support for the sending-end AC system during faults.

4) A transient voltage support strategy based on coordinated control of the LCC and MMC is proposed. In steady state, the reactive power is supported by the MMC and reactive power compensation devices. In transient state, the reactive power consumption of the LCC is adjusted to ensure maximum MMC reactive power support and transient voltage support.

5) Faults in the sending-end AC system or DC system can cause the MMC's active power to decrease, while increase its reactive power margin. The transient overvoltage mechanism of the sending-end AC system caused by DC fault will be further studied, while an MMC dynamic reactive power regulation strategy that can cope with voltage fluctuation will be proposed.

ACKNOWLEDGMENT

Not applicable.

AUTHORS' CONTRIBUTIONS

Jiangshan Liu: conceptualization, software, validation, formal analysis, investigation, and writing. Fengting Li: conceptualization, writing, and project administration. Chunya Yin: conceptualization and methodology. Lu Han: data curation. Gaohang Zhang: visualization. Ruikang Chen: checking and amending. Wan Liu: checking. All authors read and approved the final manuscript.

FUNDING

This work is supported by the National Key Research and Development Program of China (No. 2021YFB1507001).

AVAILABILITY OF DATA AND MATERIALS

Not applicable.

DECLARATIONS

Competing interests: The authors declare that they have no known competing financial interests or personal relationships that could have appeared to influence the work reported in this article.

AUTHORS' INFORMATION

Jiangshan Liu received the B.S. and Ph.D. degrees in electrical engineering from the Xinjiang University, Urumqi, China, in 2019 and 2025. His current research focuses on stability and control of hybrid cascaded HVDC system.

Fengting Li received the B.S. degree from the Beijing Institute of Technology, Beijing, China, in 1986, and the M.S. and Ph.D. degrees from Xinjiang University Urumqi, China, in 1996 and 2011 respectively. During 2008–2009, she was with Tsinghua University, Beijing, China, as a Western Light Visit Scholar. She is currently a professor with the School of Electrical Engineering, Xinjiang University. Her main research interests include power system protection power system optimization, and electric market.

Chunya Yin received the B.S. and Ph.D. degrees in electrical engineering from the School of Electrical Engineering of Xinjiang University, Urumqi, Xinjiang, China, in 2016 and 2021, respectively. He is an associate professor with the School of Electrical Engineering of Xinjiang University. His current research focuses on stability and control of AC/DC hybrid power system.

Lu Han received the M.S. degrees in electrical engineering from the School of Electrical Engineering of Xinjiang University, Urumqi, Xinjiang, China, in 2017. She is a lecturer with the School of Electrical Engineering of Xinjiang University. She is currently working toward the Ph.D. degree in electrical engineering. Her current research focuses on stability and control of AC/DC hybrid power system.

Gaohang Zhang received the B.S. degree in power and energy engineering and the Ph.D. degree in electrical engineering from Xinjiang University, Urumqi, Xinjiang, China, in 2016 and 2022, respectively. He is currently working as an associate professor with the School of Electrical Engineering, Xinjiang University. His current research focuses on stability and control of AC/DC hybrid power system.

Ruikang Chen received the M.S. degrees in electrical engineering from the School of Electrical Engineering of Xinjiang University, Urumqi, Xinjiang, China, in 2021. He is currently working toward the Ph.D. degree in electrical engineering. His current research focuses on stability and control of AC/DC hybrid power system.

Wan Liu received the B.S. degrees in electrical engineering from the School of Electrical Engineering of Jiangsu Normal University, Xuzhou, Jiangsu, China, in 2021. He is currently working toward the Ph.D. degree in electrical engineering. His current research focuses on stability and control of AC/DC hybrid power system.

REFERENCES

[1] C. Su, C. Yin, and F. Li *et al*., "A novel recovery strategy to suppress subsequent commutation failure in an LCC-based HVDC," *Protection and Control of Modern Power Systems* vol. 9, no. 1, pp. 38-51, Jan. 2024.

[2] L. Han, C. Yin, and C. Dai *et al*., "Transient voltage operational risk of a high-proportion new energy sending system," *Power System Protection and Control*, vol. 52, no. 1, pp. 23-34, Jan. 2024. (in Chinese)

[3] Y. Zhu, Y. Li, and T. Li *et al*., "Fault current analysis and active current limiting strategy for hybrid cascaded LCC/MMC HVDC system," *International Journal of Electrical Power & Energy Systems*, vol. 151, Sept. 2023.

[4] C. Hu, Y. Tong, and J. Jing *et al*., "Research on steady state control strategies of wind farm integration by VSC-LCC hybrid HVDC transmission," *Energy Reports*, vol. 6, pp. 985-991, Dec. 2020.

[5] N. Zhang, X. Li, and Z. Zhang *et al*., "Overcurrent mechanism and suppression control for MMC arms in hybrid cascaded HVDC system," *CSEE Journal of Power and Energy Systems*, vol. 11, no. 1, pp. 306-317, Jan. 2025.

[6] W. Liang, C. Shen, and H. Sun *et al*., "Overvoltage mechanism and suppression method for LCC-HVDC rectifier station caused by sending end AC faults," *IEEE Transactions on Power Delivery*, vol. 39, no. 2, pp. 1299-1302, Apr. 2024.

[7] H. Xiao, K. Sun, and J. Pan *et al*., "Review of hybrid HVDC systems combining line communicated converter and voltage source converter," *International Journal of Electrical Power & Energy Systems*, vol. 129, Jul. 2021.

[8] C. Guo, Z. Wu, and S. Yang *et al*., "Overcurrent suppression control for Hybrid LCC/VSC cascaded HVDC system based on fuzzy clustering and identification approach," *IEEE Transactions on Power Delivery*, vol. 37, no. 3, pp. 1745-1753, Jun. 2022.

[9] J. Zhao and Y. Tao, "Hierarchical coordinated adaptive droop control for hybrid HVDC with cascaded multi-infeed MMC inverters," *IET renewable power generation*, vol. 16, no. 6, pp. 1148-1158, Apr. 2022.

[10] Y. He, W. Xiang, and B. Ni *et al*., "Impact of strength and proximity of receiving AC systems on cascaded LCC-MMC hybrid HVDC system," *IEEE Transactions on Power Delivery*, vol. 37, no. 2, pp. 880-892, Apr. 2022.

[11] J. Liu, S. Lin, and L. Xia *et al*., "Mitigation strategy of commutation failure based on reactive power feedback control in the HC-HVDC," *IEEE Transactions on*

Power Delivery, vol. 39, no. 4, pp. 2079-2091, Aug. 2024.

[12] P. Meng, W. Xiang, and Y. Chi *et al*., "Resilient DC voltage control for islanded wind farms integration using cascaded hybrid HVDC system," *IEEE transactions on power systems*, vol. 37, no. 2, pp. 1054-1066, Mar. 2022.

[13] X. Fan, Y. Chi, and Z. Wang *et al*., "Coordinated reactive power control for hybrid cascaded high-voltage direct-current links in weak AC grids," *IET generation, transmission & distribution*, vol. 18, no. 23, pp. 3788-3800, Dec. 2024.

[14] X. Fan, Y. Chi, and Z. Wang *et al*., "Frequency support scheme of grid-forming based hybrid cascaded HVDC integrated wind farms," *IET generation, transmission & distribution*, vol. 18, no. 3, pp. 446-459, Feb. 2024.

[15] C. Yin and F. Li, "Analytical expression on transient overvoltage peak value of converter bus caused by DC faults," *IEEE Transactions on Power Systems*, vol. 36, no. 3, pp. 2741-2744, May 2021.

[16] C. Yin and F. Li, "Reactive power control strategy for inhibiting transient overvoltage caused by commutation failure," *IEEE Transactions on Power Systems*, vol. 36, no. 5, pp. 4764-4777, Sept. 2021.

[17] H. Gong, J. Guo, and Q. Guo *et al*., "Overvoltage calculation method for sending system under DC fault disturbance considering the influence of renewable energy," *CSEE Journal of Power and Energy Systems*, vol. 10, no. 5, pp. 1865-1875, Sept. 2024.

[18] J. Liu, F. Li, and C. Yin *et al*., "Mechanism of and suppression strategy for transient voltage fluctuation in the commutator bus of a hybrid cascaded DC system caused by commutation failure," *Power System Protection and Control*, vol. 51, no. 20, pp. 36-46, Oct. 2023. (in Chinese)

[19] X. Ma, F. Li, and C. Yin *et al*., "Impact of voltage restoration of commutation bus on rectifier side on commutation of inverters," *Power System Technology*, vol. 44, no. 8, pp. 2950-2960, Aug. 2020. (in Chinese)

[20] Y. Shi, C. Yin, and F. Li *et al*., "Transient overvoltage mechanism and control strategy considering active and reactive interaction when there is a fault in the sending end AC system," *Power System Protection and Control*, vol. 52, no. 21, pp. 117-128, Nov. 2024. (in Chinese)

[21] T. Wang, L. Pei, and J. Wang *et al*., "Over-voltage suppression under commutation failure based on improved voltage-dependent current order limiter control strategy," *IEEE Transactions on Industry Applications*, vol. 58, no. 4, pp. 4914-4922, Jul. 2022.

[22] Q. Xie, X. Xiao, and Z. Zheng *et al*., "An improved reactive power control strategy for LCC-HVDC to mitigate sending end transient voltage disturbance caused by commutation failures," *International Journal of Electrical Power & Energy Systems*, vol. 146, Mar. 2023.

[23] Y. Li, Y. Zeng and W. Zhang *et al*., "Coordinated optimization method for suppressing transient overvoltage caused by HVDC commutation failure considering large wind power integration," *Energy Reports*, vol. 9, pp. 1171-1182, Dec. 2023.

[24] X. Jin and H. Nian, "Overvoltage suppression strategy for sending ac grid with high penetration of wind power in the LCC-HVDC system under com-mutation failure," *IEEE Transactions on Power Electronics*, vol. 36, no. 9, pp. 10265-10277, Sept. 2021.

[25] Z. Zheng, J. Ren and X. Xiao *et al*., "Response mechanism of DFIG to transient voltage disturbance under commutation failure of LCC-HVDC system," *IEEE Transactions on Power Delivery*, vol. 35, no. 6, pp. 2972-2979, Dec. 2020.

[26] Z. Zeng, J. Zhao, S. Zhang *et al*., "Sensitivity analysis of different controller parameters on the stability of the weak-grid-tied interlinking VSC," *Protection and Control of Modern Power Systems*, vol. 10, no. 6, pp. 40-51, Jan. 2025.